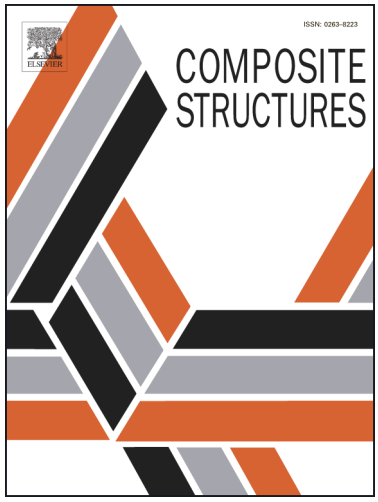

An Experimental Investigation into The High Velocity Penetration Resistance of CFRP and CFRP/Aluminium Laminates

Ming-ming Xu, Guang-yan Huang, Yong-xiang Dong, Shun-shan Feng

PII: S0263-8223(17)32911-2
DOI: https://doi.org/10.1016/j.compstruct.2018.01.020
Reference: COST 9260

To appear in: *Composite Structures*

Received Date: 8 September 2017
Revised Date: 29 November 2017
Accepted Date: 9 January 2018

Please cite this article as: Xu, M-m., Huang, G-y., Dong, Y-x., Feng, S-s., An Experimental Investigation into The High Velocity Penetration Resistance of CFRP and CFRP/Aluminium Laminates, *Composite Structures* (2018), doi: https://doi.org/10.1016/j.compstruct.2018.01.020

An Experimental Investigation into The High Velocity Penetration Resistance of CFRP and CFRP/Aluminium Laminates

Ming-ming Xu, Guang-yan Huang*, Yong-xiang Dong, Shun-shan Feng

State Key Laboratory of Explosion Science and Technology, Beijing Institute of Technology, Beijing 100081, P. R. China

Abstract: Carbon fibre-reinforced composite materials are of high potential as protective casing in the aerospace area, acting as an effective solution to lighten components against the collision. The high velocity penetration resistance abilities of unidirectional CFRP laminates and two carbon fibre reinforced aluminium laminates CRALL2/1 and CRALL3/2 (fabricated from CFRP layers combined with aluminium alloy 2024-T3 layers) were evaluated by the ballistic tests with a flat, hemispherical or conical nosed projectile. Revealed from ballistic tests that fracture modes, ballistic limits and specific energy absorptions of CRALLs and CFRP were sensitive to nose shapes. Higher ballistic limits and specific energy absorption ability were performed by CRALLs than monolithic CFRP impacted by all shapes due to the strain rate hardening effect and failure conversion effect. In particular situation of flat nose projectiles penetrating, the specific energy absorption of the CRALL3/2 was 8% higher than that of monolithic aluminium alloy 2024-T3 at same thickness. The CRALLs may then be designed as effective lightweight structures to protect frames against collision in the aerospace area and outperform the traditional single CFRP

* Corresponding author.

E-mail address: huanggy@bit.edu.cn (Guang-yan Huang).

laminates.

Keywords: Fibre metal Laminates; Carbon fibres; Impact behaviour; Fracture

1. Introduction

Carbon fibre reinforced aluminium laminates (CRALL) are a kind of fibre-metal laminates (FMLs) materials combining the excellent impact resistance of metallic materials with the good fatigue behaviour of fibre reinforced polymeric (FRP) materials. FMLs are an advanced hybrid materials system being evaluated as a damage tolerance and light weight solution for aircraft primary structures due to their increased stiffness and strength in comparison to aluminium.

The impact response of fibre-metal laminates, in particular, formed by imbedding glass and aramid fibre in aluminium laminates (GLARE and ARALL), have received much attention from recent experimental studies and are presently being employed in aviation applications [1, 2]. Examples such as GLARE panels in the upper fuselage of the Airbus A380 commercial aircraft and ARALL panels to be used as material for the highly fatigue rear cargo door of the C-17 cargo door to reduce overall weight [3, 4]. In fact, sufficient experimental data have been generated, demonstrating the superior fatigue performance and impact resistance of GLARE compared to monolithic aluminium alloys [5-8]. In the alternatives, researches on the impact behaviour of the CFRP and CRALL have been performed mainly in static and low velocity regimes (<10 m/s). Till now, insufficient experimental results can be found in literatures that described in detail in the impact resistance of CFRP and

CRALLs for high velocity regimes (>100 m/s). One probable reason may be due to the poor damage resistance of CFRP and CRALL in the low energy drop weight tests [6], other reasons probably due to the cost of high velocity investigations and measuring difficulty.

A number of experimental papers have compared the damage and fracture prevention properties of glass, aramid and carbon fibre reinforced materials. These investigations have been early discussed in detail in the report by Vlot A in 1990s [7], where the low velocity impact and static indentation tests were conducted on the GRALL, ARALL, CFRP and CARE (made of Al 2024/carbon 0°/Al 2024) with approximate equal areal density (3.4 kg/m^2), punctured by same hemispherical tipped impactors. Results showed that the carbon laminates (CFRP and CARE) performed lowest energy absorption ability to resist a through crack than glass and aramid fibre reinforced metal laminates due to its low strain to failure (< 2%).

Then a series of studies followed Vlot's experimental program were carried out on the glass, aramid and carbon fibre reinforced metal laminates. The results of which however, are subject to some low velocity discussion. For example, Caprino G et al. [8] performed low-velocity impact tests on GLARE composites made of Al 2024-T3 sheets and S2-glass/epoxy prepreg layers and showed that the overall force–displacement curves only depended on the impact energy, rather than on the mass and speed separately. Results showed that GLARE offered better performance in terms of penetration energy and damage resistance than aramid fibre-reinforced

laminates. The high velocity impact tests on GLARE panels were also performed by Hoo Fatt et al. [5] with a blunt cylinder projectile to build an analytical solution to predict the ballistic limit and energy absorption of GLARE panels.

On the CRALL side, Dhaliwal GS et al. [4], Yu GC et al. [9], and Bieniaś J et al. [10] studied the load-time history curves and failure mode of the Al/CFRP laminates made of various fibre directions ([0°], [±45°] and [0°/90°]) under low energy impacting (from 10 J to 31 J, less than 5 m/s). Results showed an upward trend of the highest value of load force with the increasing impact energy. Also, the ply configuration in Al/CFRP laminates has particularly importance for their impact resistance as the FMLs with the orthogonal ([0°/90°] and [±45°] ply sequences) carbon fibre laminates performed the best impact resistance behaviour followed by the unidirectional ([0°] ply sequences) laminated configurations. Also, a series of ballistic impact tests have been performed on CFRP with several specified structures [11-13]. For example, the satin weave carbon/epoxy laminates of 3.2 mm and 6.5 mm in thickness were penetrated by projectiles with geometries representing hemispherical, conical, fragment simulating and flat tip in Ulven C. et al. [11]. Results showed that the impact fracture mode of satin weave carbon/epoxy laminates were insensitive to the projectile tips. Contrarily, results of the high velocity penetration tests on thin carbon/epoxy woven laminates performed by López-Puente J et al. [12,13] using a gas gun showed that the fracture mode was both affect by projectile tips and initial velocity. Different analytical models corresponding to projectile shapes

were developed to predict the residual velocity.

These previous impact and static indention test results of various fibre and corresponding fibre mental laminates are summarized and compared in Fig. 1 with an approximate equal areal density. Considering different thickness planet, fibrous type, dimension and mass of impactors, ratio between projectiles and targets were adopted in these experimental tests of various literatures [5-12], the specific cracking energy $U_{spec.} = E_{\min} / \rho_d$ (J·m^2/kg) is employed to roughly evaluate the penetration resistance levels, which is the minimum energies $E_{\min}$ recorded divided by area density ρ_d to create the through crack in the materials [7]. As shown in Fig. 1, the CFRP or CRALL exhibited the lowest specific cracking energy under static, low velocity or high velocity impact loading. However, the GLARE exhibited the highest specific cracking energy, even outperform monolithic aluminium under higher velocity impact loading [5]. May be due to the lowest failure energies under static and low velocity penetrations, the CRALL has received less attention than glass and aramid fibre reinforced aluminium laminates. Also, few researches have employed drop weight test to study the low velocity impact response of CRALL [6-10], and yet insufficient experimental data have been reported on penetration resistance of CRALL at high velocity exceeding 10 m/s.

However, as it shown in Fig. 1, the specific cracking energies of FMLs showed an increasing trend under the higher velocity impacting. This can be related to the strain rate hardening behaviour of the materials, also more energy dissipation at high

velocity due to vibrations [6]. It has been reported recently that, the CRALLs were also strain rate sensitive materials, even though the carbon fibre was strain rate insensitive [14-16]. For example, the tensile behaviours of a 3/2 lay-up CRALL (made of three layers aluminium 2024-T3 sheet bonded by two layers unidirectional CFRP-T300) determined at strain rate from 0.001 s^{-1} to 1200 s^{-1} showed that both the ultimate tensile strength and failure strain of the CRALL increased with higher strain rate [14, 15].

These tensile stress–strain curves of CRALLs [14] are compared to these of unidirectional CFRP-T300 [17] and aluminium 2024-T3 [18], in Fig. 2, The shaded areas (kJ/m^3) under the stress–strain curves evaluate the crack energy absorbing ability of the specimens while deforming to breaking. Under quasi-static rate, the crack energy of unidirectional CFRP-T300 exhibited the minimum value 12.3×10^3 kJ/m^3 due to the small breaking strain (less than 2%), the aluminium 2024-T3 acquired the highest value 42.1×10^3 kJ/m^3 due to its better ductility. The crack energy of CRALL 3/2 before rupture was 21.4×10^3 kJ/m^3, less than that of aluminium 2024-T3 but higher than CFRP. Under strain rate of 1200 s^{-1}, the crack energy of CRALL 3/2 was 51.6×10^3 kJ/m^3, approximately 22% higher than that of the aluminium 2024-T3. This strengthening effect was predicted by a linear strain hardening model combined with Weibull distribution function [14, 15]. From these related studies, the CRALLs can be verified as the strain rate sensitive material and exhibit increasing ductility and strength especially under high strain rate whereby

higher energy absorption capability can be performed by CRALLs under high velocity impact loading.

In addition, plenty of effective enhancement technologies have been reported to improve the penetration resistance of CRALLs, such as increasing the yield strength of face aluminium sheets [9], improving the interlaminar mechanical properties of CRALLs [19], forming the carbon-fibre core into honeycomb and sandwich structures [20], which are promoting innovative solutions to lighten aircraft primary structures.

Based on these concepts, an experimental investigation to examine the high velocity penetration resistance of the CFRP and CRALLs under projectiles impacting have been completed in this paper. These 4 mm thick CFRP targets were made of orthogonal T700S laminates. These targets of 2.48 mm thick CRALL3 (2/1 layup) and 4.16 mm thick CRALL5 (3/2 layup) configurations were made of 0°/90° CFRP-T700S layers bonded by aluminium alloy 2014-T3 face sheets with adhesive prepreg. These projectiles with a flat, hemispherical or sharp nose were accelerated to 80~250 m/s using the air gun. The influence of the projectile nose shape on the impact behaviours of the CFRP and CRALLs plates were analysed in detail through penetrating process captured by high-speed cameras and the cross-section surfaces of targets after penetration. The ballistic limits and energy absorption ability of CFRP laminates, CRALLs and monolithic aluminium alloy 2014-T3 plates were also compared with similar thickness in the ballistic impact test.

2. Materials of impact specimen

2.1. Cross-ply CFRP

As shown in Fig.3, the CFRP target panels in this paper were orthogonally laminated at elevated temperature by unidirectional T700S fibre prepregs with epoxy-base adhesive, produced by Toray Industries, Inc., Japan. These unidirectional T700S prepregs were 100 g/m^2 in gram weight and 0.1 mm in thickness. The fibre volume fraction in the CFRP composite was 60%. These 4 mm thick monolithic cross-ply CFRP laminates were comprised of 40 plies in [0°/90°] orthogonal position and these 0.8 mm thick cross-ply CFRP laminates used in CRALL were comprised of 8 plies in [0°/90°] orthogonal position. The static properties of the unidirectional T-700S fibre prepreg taken from the manufacturer [17] and reference [21] are given in Table 1.

2.2. Aluminium alloy 2024-T3

The traditional aluminium alloy 2024-T3 which is widely adopted in aerospace was employed because of its high ductility and lightweight. In CRALLs, the Al 2024-T3 sheets were bonded to cross-ply CFRP laminates as front and rear face sheets to reduce the initial impact damage in the CFRP. Meanwhile, these 2.5 mm and 4 mm thick monolithic Al 2024-T3 were penetrated in the ballistic impact tests as a comparative evaluation to the effectiveness of CRALLs on the penetration resistance and energy absorption at equal thickness. The mechanical properties of Al 2024-T3 are listed in Table 2 [18].

2.3. CRALLs Lay-up configuration

These CRALLs were designed based on the fibre-metal laminate concept of commercially available GLARE for the usage in impact-prone structures [5]. These two CRALL configurations: the 2/1 lay-up sequence, with one layer of 0.8 mm thick T700S CFRPs bonded by two layers of 0.8 mm thick Al 2024-T3 sheets; and the 3/2 lay-up sequence, with two layers of 0.8 mm thick T700S CFRP bonded by three layers of 0.8 mm thick Al 2024-T3 sheets. The off-white epoxy adhesive DP460, produced by 3M™ Scotch-Weld™, was used to bond the CFRP layers and the aluminium layers together. As shown in Fig.4, with the addition thickness of adhesive layers, the total thickness of the two types CRALLs were approximately 2.48 mm and 4.16 mm, respectively.

3. Impact experiments setup

The impact tests were conducted at room temperature using the air gun, which was upgraded from a SHPB test platform to ensure the coaxiality and normal impact angle. Recorded by the high-speed photography, the deflection angles of the projectiles were less than 5°. The 2 m long gun barrel had an inside diameter of 16 mm. The air gun consisted of a pressure vessel with a pressure capacity of 20 MPa, which can accelerate the 30 g steel projectile up to 80~350 m/s. The 130×130 mm square targets panels were fixed to the support by the steel clamping ring with twelve M6 blots. As shown in Fig.5, the circular impact area had a diameter of 100 mm. The

specimen supporting plate was mounted to a steel box and oriented normal to the gun barrel. The steel box was designed to collect any possible fragments detached from the targets.

The high-speed camera system (Phantom V710) was applied to record the velocity, impact conditions and maximal range of striking angle. The initial impact velocity v_i, and the residual velocity v_r, were determined by $v = \Delta d / \Delta t$, where Δd was the displacement of the projectile between two frames and Δt was the recorded time interval. The frame rate was 45,000 fps and the resolution was 550×300 pixels.

The 45# steel cylinder projectiles with a tip of flat, hemisphere or sharp nose had identical 16 mm diameter. For each tip geometries, the lengths of the projectiles were adjusted slightly to ensure the consistent total 30 g in mass. The impact tests were classified by labels F, H, and S for flat, hemisphere, and sharp nose projectiles. These short labels of CF4, CRALL3, CRALL5, Al2 and Al4 represent 4 mm CFRP, 2.48 mm CRALL2/1, 4.16 mm CRALL3/2, 2.5 mm Al 2024-T3 and 4 mm Al2024-T3.

4. Results and discussion

4.1. Impact performance cross-ply laminated CFRP

4.2.1 Deformation and failure process penetrated by flat nose projectile

In Fig.6, the 4 mm CFRP target was totally penetrated by the 152 m/s (346 J) flat nose projectile with massive long fibre bundles were peeled off the last layer. At about

874 μs, the localized bulge on the backside formed caused by the projectile. Meanwhile, the transverse impact compressive wave reflected as a tensile one on the free-interface was causing initial fibre spalling. When the projectile thoroughly penetrated the CFRP target at about 1000 μs, the shear plug was formed in front of the projectile nose. Meanwhile, with the longitudinal tensile wave propagated to the fixed boundary, the fibre bundles of the last layer were broken and delaminated off the laminated CFRP target. The shear fracture and delamination phenomenon were unique and quite different from these results of weave CFRP, which no shear plug was formed but mainly tensile fracture [11-13]. Although mainly shear fracture of the CFRP laminates was caused by high-velocity flat nose projectile, there was also tensile fracture caused on the rear part if the velocity lowed enough. In Fig. 7, after 106 m/s penetration, the most forepart of the target was shear fracture, while the rear part were mainly tensile fracture due to these fibre plies had enough time to bend. It can be summarized that both impact velocity and fabric architectures will affect the fracture mode of CFRP by flat nose projectile.

In Fig. 7(a), the radius of the shear hole of penetrated CFRP by 152 m/s flat projectile was approximately 14.9 mm, close to the radius of the projectile body. Around the impact area, there was interlayer breakage between the first and second plies due to the low specific fracture energy of epoxy matrices. No obvious delamination failure alongside the shear fracture face, except the massive fibre bundles delamination of the last plies due to the tensile failure. The lamellated shear

plug collected indicated the compressive delamination failure in the shear plug under projectile compression.

4.2.2 Deformation and failure process impacting by hemisphere nose projectiles

In Fig. 6, the 4 mm thick CFRP target was thoroughly penetrated by 149 m/s (333 J) hemispherical nose projectile. At 1125 μs, when the hemispherical nose projectile partly penetrated into the CFRP target, fibre bundles began to break and peel off from the last fibre ply. Different from the flat nose projectile, there was no plug formed. Approximately at 1292 μs, the projectile fully penetrated through the CFRP target.

As shown in Fig. 7(b), mainly tensile cross cracks were caused by hemispherical nose projectile near the ballistic limit velocity, which were along and perpendicular to the fibre direction, resulting in both fibre and matrix tensile failure in the penetrated area. The crushed indentation on the impacted surface indicated compressive damage caused by the concentrated stress around the projectile nose. The rhombic shaped bulge area was formed on the backside due to the orthogonal tensile cracks in the penetrated area. The delamination appeared in the first fibre plies, back fibre plies and severely alongside the cross cracks due to the interlayer shear failure. As shown in Fig. 6, besides long fiber bundles, these short fibre debris pulled out from the last layers were too small to be collected.

These tensile fractures caused by hemispherical projectile coincided those woven

CFRP in static and impact tests [11]. This does not consequently imply the fracture mode caused by hemispherical nose impactor is insensitive to the impact velocity. Under hypervelocity impacts, for example up to 1 km/s [22], the CFRP were crushed into fibre debris cloud as the initial contact compressive stress wave was strong enough to crush the fibre through the thickness before bending.

4.2.3 Deformation and failure process impacting by sharp nose projectiles

The penetrating process of CFRP target by sharp nose projectile is rarely reported. In this study, these conical nose projectiles with a 90° cone angle were used. In Fig. 6, the 4 mm CFRP target was thoroughly penetrated by 145 m/s (315 J) sharp nose projectile with massive long fibre bundles peeled off and small short fibres pull out from the fibre plies in which no plugs formed.

This penetration process resembled the fracture feature of hemispherical nose projectile. As shown in Fig. 7(c), mainly tensile orthogonal cracks were caused by sharp hemispherical nose projectile near the ballistic limit velocity with shear failure delamination involved. Under 70 m/s impacting, the crushed indention on the impacted surface, as well as the backside bulge, was caused by the shape tip, with initial tensile cracks spread into interlayers. Under higher velocity of 145 m/s, the tensile cracks fully penetrated through the thickness with severely delamination alongside the cross cracks due to the interlayer shear failure. The sharp nose was punching into the fibre layers and pushing aside the fibres, resulting in a reverse bulge

area uplifted on the front side and rhombic bulge shaped on the back side. Despite the reverse bulge area, these similar fracture surfaces by hemispherical and sharp projectiles maybe due to their geometries. The major difference relied on the ratio between the tensile and shear failure involved between two projectiles penetrating.

4.2.4 Penetration resistance of CFRP under out-of-plane impact

The penetration resistance performance of CFRP targets to high velocity projectiles were evaluated by the ballistic limits and energy absorption ability. There are also analytical models to predict the residual and the ballistic limit velocities by global response analysis of each system and balance approach or principles of moment conservation [5, 12, 23, 24]. Most of these models have been developed with acceptable accuracy using flexible laminates of glass, aramid or polyethylene fibres. A smaller number of impact models consider carbon laminates subjected to high-speed impact [13]. These analyses provide algebraic or differential equations whose solutions are of value in only isolated situations. The necessary simplifications to consider in these models means that they are useful only for the problem for which they were derived. One example is the analytical models [23] overestimated the ballistic limit of woven carbon laminates under high velocity impacting by as much as 20% to 43% due to specific failure mechanisms and weave architectures [11].

Considering the uniform standard and validity for various fracture modes in the cross-ply CFRP by each projectile shape, the more practically used in terminal

ballistic Lambert–Jonas approximation was employed, as a class of models describing penetration phenomenon was found which imply Lambent–Jonas correlation between the impact, the residual and the ballistic limit velocities [25]:

$$v_r = a(v_i^{\,p} - v_{bl}^{\,p})^{1/p}, \quad (1)$$

where v_i, v_r and v_{bl} were initial, residual and ballistic limit velocities, p and a are coefficients. The ballistic limits v_{bl} of the 4 mm cross-ply CFRP were obtained from the fitting curves in Fig. 8 (these negative residual velocities are representing velocities of bounce back projectiles).

From fitting curves in Fig. 8(a), it showed that the 4 mm cross-ply CFRP target performed the highest penetration resistance to flat nose projectile, and relatively lower penetration resistance to hemispherical and sharp nose projectiles. These ballistic limits corresponding to flat, hemispherical and sharp nose projectile were 90.30 m/s, 76.13 m/s and 73.87 m/s. The ballistic limit of 4 mm CFRP to flat nose projectile impacting was 19% and 22% higher than to hemispherical and sharp nose projectile impacting. The hemispherical and sharp nose projectile penetrates with lower ballistic limits because they initially created the compressive crush zone followed by elastic tensile rupture enlargement where the orthogonal cracks were more likely to spread and stretch while the projectile penetrates. The flat nose projectile also created compressive stress accompanied with shear plugging during impact, but the energy absorbed was much greater due to the large impact face.

As in Fig. 8(b), the kinetic energy loss of the flat nose projectiles after penetration was higher than 122.31 J (at the ballistic limit velocity), and showing a slightly increasing trend with the raise of the initial impact velocity. Due to similar deformation and fracture modes during penetration, the ballistic limit fitting curve and the kinetic energy loss of the hemispherical and sharp nose projectiles were convergent and overlapped at high values of initial velocities. The kinetic energy loss of the hemispherical and sharp projectiles were roughly constant over high value of initial velocity, around the 86.93 J and 81.85 J (kinetic energy loss at the ballistic limit velocity), fluctuating within 7%. These horizontal trends in kinetic energy loss maybe due to the consistent bending deformation and fracture mode during a specific impact velocity region.

4.3. Penetration performance of CRALLs

4.3.1 Deformation and failure process of the CRALL2/1 targets

Due to the poor mechanical property and low stress wave impedance of adhesive layers [26], the Al sheets and fibre layers of CRALLs were completely debonded under impacting. To determine the magnitude of the adhesive debonding effect contributed to the penetration resistance of the multi-layered target is associated with extra systematic investigations using numerical and experimental approaches involved with bonding situations (free, low strength and high strength adhesive) and failure modes (interlayer shear failure, out-of-plane shear or in-plane Shear). The debonding

effect couldn't be fully assessed from present study as it all completely debonded. So, the emphasis has been placed on the effect of projectile nose shape on the fracture mode of each layer in CRALLs during ballistic tests.

These typical fracture modes of CRALL2/1 targets after projectiles penetration were summarized in Fig. 9. Under 109.6 m/s flat nose projectile impacting, mainly shear damage was caused through the thickness. The residual deformations of the front Al face sheet and fibre interlayer were localized. The back Al sheet performed relatively larger residual deformation with both shear and tensile failure. These approximate orthogonal cracks on the Al sheet resembled cracks directions in the fibre interlayer.

Under 106.9 m/s hemispherical nose projectile impacting, the front Al fact sheet was featured with localized ductile hole fracture. The perforated hole was approximately 13.6 mm wide on the front Al face sheet and 9.8 mm deep measured by depth indicator. The tensile damage in the fibre interlayer resulted in two orthogonal cracks in the centre, approximately 45 mm in length each. Induced by this 0°/90° cracks, the back Al face sheet also fractured in orthogonal tensile cracks with the diamond shaped bulge, approximately 15.3 mm below the original surface.

Under 102.8 m/s sharp nose projectile impacting, the fracture modes of each layer resembled those under hemispherical nose projectile impacting. The perforated hole on the front Al face sheet was approximately 10.4 mm in deep. The orthogonal cracks on the [0°/90°] fibre interlayer was approximately 49 mm in length each. On

the back Al face sheet, the nadir of the diamond shaped bulge caused by orthogonal tensile cracks was approximately 17.6 mm below the original surface.

It obvious that impact behaviours of CRALL2/1 were significantly affected by projectile shapes, as shown in Fig. 9. Meanwhile, comparing the localized fracture of front Al sheet and monolithic Al targets to that of the back Al sheet in CRALL2/1 in Fig. 9, it showed an obvious failure conversion effect, where the orthogonal fibre laminates had transformed the localized fracture (shear plugging or ductile holing) of front Al sheets into dishing tensile cracks of back Al sheet, induced by orthogonal cracks in the fibre interlayer conversing the concentrated stress around projectile tip into membrane stretching of the back Al face sheet during penetrating.

4.3.2 Deformation and failure process of the CRALL3/2 targets

The typical fracture modes of CRALL 3/2 targets under projectiles impacting were summarized in Fig. 10. After 175.9 m/s flat nose projectile penetration, mainly shear plugging fracture on the first aluminium layer and second fibre layer, and transformed into hybrid fractures with shear and tensile failure in residual three layers. Under flat nose projectile penetration, this failure conversion effect caused by the 0°/90° CFRP interlayers in CRALL3/2 were more obvious than that in CRALL2/1, as the shear fracture in the 2^{nd} fibre layer had been transformed into tensile cracks in the 4^{th} fibre layer in CRALL3/2 target.

After approximate 175 m/s penetration, similar bend deformations and fracture

modes were performed by CRALL3/2 targets when penetrated by hemispherical and sharp nose projectiles: the localized ductile hole fracture on the first Al face sheets resembled the fracture surface of the monolithic 4 mm thick Al plates; the concentrated stress of the projectile tip resulted in initial crushing breakage in the second fibre layers and the movement of the projectile cracked the fibre and matrix; mainly tensile fracture were performed in the last three layers in the CRALL3/2 target, with orthogonal cracks and the diamond shaped bulge on the backside.

In CRALL2/1 and CRALL3/2 targets, the failure conversion effect induced by the [0°/90°] fibre interlayer converting the fracture modes of front and back layers were obvious. As the [0°/90°] carbon fibre interlayers were continually conversing the concentrated stress around projectile tip into membrane stretching of the next layers, this effect diminished the influence of the projectile shapes on fracture modes in CRALLs with the increasing number of the multi-layers, evidence such as these backside layers in CRALL3/2 performed analogous tensile fracture to the projectiles penetration with three nose shapes.

4.3.3 Penetration resistance of CRALLs

The penetration resistance performance of CRALL targets to high velocity projectiles penetration were evaluated by the ballistic limit and the energy absorption ability, summarised in Table 4 and Fig. 11 (these negative residual velocities are representing velocities of bounce back projectiles). The ballistic limits of 2.48 mm

thick CRALL2/1 were 85.2 m/s by flat nose projectile, 80.9 m/s by hemispherical nose and 70.8 m/s by sharp nose projectile. The ballistic limit of flat nose projectile was 5% and 20% higher than that of hemispherical and sharp nose projectile. Similarly, the ballistic limit of 4.16 mm thick CRALL3/2 was 121.1 m/s by flat nose projectile impact, 13% and 10% higher than that of hemispherical and sharp nose projectile. This was correlated to larger impact face of flat nose projectile during penetration than that of hemispherical and sharp nose projectile which resulted in more energy absorbed. Due to similar fracture modes at high value of initial velocity under hemispherical and sharp nose projectiles penetration, their ballistic limit fitting curves of CRALL2/1 and CRALL3/2 overlapped when far above the ballistic limits.

In Fig. 11(c), the average kinetic energy loss of the flat nose projectile after penetrated the CRALL2/1 targets was 117.1 J, approximately 23% higher than that of hemispherical nose projectiles and 43% higher than that of sharp nose projectiles. However, the energy absorption abilities of CRALL2/1 targets to three shapes nose projectiles were still lower than monolithic Al 2024-T4 targets at similar thickness. In Fig. 11(d), the average kinetic energy loss of the flat nose projectiles after penetrated the CRALL3/2 targets was 235.8 J, approximately 48% higher than that of hemispherical nose projectiles and 32% higher than that of sharp nose projectiles. Comparing the CRALL3/2, CFRP and monolithic Al 2024-T4 targets at 4 mm thickness, to all three shapes projectile, the energy absorbed by CRALL3/2 targets was higher than CFRP, but also lower than monolithic Al 2024-T4 targets.

4.4. Penetration resistance enhancement of CRALLs

4.4.1 Ballistic limits

The penetration resistance properties of the CFRF, CRALLs and Al 2014-T3 targets were summarised in Table 4. Results showed that the ballistic limits of the CRALL3/2 were far higher than that of the CFRP targets at similar 4 mm thickness, approximately 40% above. However, the ballistic limits of the CRALLs were still lower than Al 2014-T3 targets at 2.5 mm and 4 mm thicknesses. Considering the mass of the targets, the ballistic limit trend lines of all 5 targets types in various areal weight density were compared in Fig. 12. The trend line of CRALLs targets impacted by flat nose projectile was above the trend lines of hemispherical and sharp nose projectiles at same areal weight density. Though the CRALL3/2 targets performed higher ballistic limits than monolithic CFRP targets, the ballistic limits of the CFRP targets still fell on the trend lines of the CRALLs targets in the ballistic limit to areal weight density coordinate when impacted by flat and sharp nose projectiles.

4.4.2 Energy absorption ability

Another parameter important to evaluate penetration resistance of materials is the specific energy absorption $\Delta\bar{E}_e$, here it is defined as:

$$\Delta\bar{E}_e = \frac{1}{\rho d}\frac{\Delta E_{k1} + \cdots \Delta E_{ki} \cdots + \Delta E_{kn}}{n}, \tag{2}$$

where ρ and d are the equivalent density and total thickness of the targets, ΔE_{ki} is the kinetic energy loss of the projectile after penetrated the targets, n is the number of the

reparations of fully penetrated cases.

In Fig. 13, under hemispherical and sharp nose projectiles penetrating, the monolithic Al 2024-T4 targets exhibited highest specific energy absorption ability and the monolithic CFRP targets performed the lowest one. Particular situation occurred under flat nose projectiles penetrating, as shown in Fig.13(a), though in Fig.12, the ballistic limit trend lines in CRALLs targets impacted by three shapes nose projectiles were lower than those of monolithic Al 2024-T4 targets at same areal weight density, however, when considering the energy absorption ability, the specific energy absorption of the 4.16 mm thickness CRALL3/2 targets are 17% higher than that of 4 mm thickness CFRP targets and 8% higher than that of 4 mm thickness Al 2024-T3 targets. Ignore the extra 0.16 mm thickness of low strength adhesive layers, the CRALL 3/2 targets was comparable with the monolithic aluminium targets, benefited from its strain rate hardening effect and non-localized membrane stretched deformation due to the failure conversion effect. As shown in Fig.13(b) and (c), even though still lower than monolithic Al 2024-T4 targets at similar thickness, the specific energy absorption of 4.16 mm thick CRALL3/2 targets was increased by 37% and 52% respectively comparing to that of 4 mm thick CFRP targets penetrated by hemispherical and sharp nose projectiles.

5. Conclusions

The high velocity penetration resistance ability of the CFRP and CRALLs targets

have been investigated by the projectiles with a flat, hemispherical or sharp nose. Also compared with the monolithic aluminium 2024-T3 targets at same thickness. These conclusions can be draw below from the comparison:

Under high velocity impacting, the fracture modes of the orthogonally laminated CFRP and CRALLs targets are sensitive to projectile nose shapes. With the increasing fibre layers, the influence of the projectile nose shapes on fracture modes of the backside layers in the CRALLs will be diminished by the failure conversion effect.

The CRALLs targets performed better penetration resistance to the three shapes nose projectiles than CFRP both in aspects of the ballistic limits and energy absorption performance due to the strain rate hardening effect.

The CFRP and CRALLs targets performed better penetration resistance to flat nose projectile than to hemispherical sharp nose projectiles. The specific energy absorption of CRALL3/2 to flat nose projectile was 8% higher than that of monolithic aluminium alloy 2024-T3 at similar thickness.

Acknowledgements

This work was supported by National Natural Science Foundation of China [No. 11772059], [No.11472053]; and the Foundation of State Key Laboratory of Explosion Science and Technology of China [No. KFJJ13-1Z].

References

[1]. Sadighi M, Alderliesten RC, Benedictus R. Impact resistance of fiber-metal laminates: A review. Int J Impact Eng 2012;49:77-90.

[2]. Chai GB, Manikandan P. Low velocity impact response of fibre-metal laminates - A review. Compos Struct 2014;107:363-81.

[3]. Vlot A, Vogelesang LB, de Vries TJ. Towards application of fibre metal laminates in large aircraft. Aircr Eng Aerosp Technol 1999;71(6):558-70.

[4]. Dhaliwal GS, Newaz GM. Modeling Low Velocity Impact Response of Carbon Fiber Reinforced Aluminum Laminates (CARALL). J Dyn Behav Mater 2016;2(2):181-93.
[5]. Hoo Fatt MS, Lin C, Revilock DM, Hopkins DA. Ballistic impact of GLARE™ fiber-metal laminates. Compos Struct 2003;61(1-2):73–88.
[6]. Vlot A. Impact loading on fibre metal laminates. Int J Impact Eng 1996;18(3):291-307.
[7]. Vlot A, Krull M. Impact Damage Resistance of Various Fibre Metal Laminates. J Phys IV, 1997, 7(C3):1045-50.
[8]. Caprino G, Spataro G, Del Luongo S. Low-velocity impact behaviour of fibreglass-aluminium laminates. Compos Part A Appl Sci Manuf 2004;35(5):605-16.
[9]. Yu GC, Wu LZ, Ma L, Xiong J. Low velocity impact of carbon fiber aluminum laminates. Compos Struct 2015;119:757-66.
[10]. Bieniaś J, Jakubczak P. Low velocity impact resistance of aluminium/carbon-epoxy fiber metal laminates. Compos Theory Pract 2012;12(3):193-7.
[11]. Ulven C, Vaidya UK, Hosur M V. Effect of projectile shape during ballistic perforation of VARTM carbon/epoxy composite panels. Compos Struct 2003;61(1-2):143-50.
[12]. López-Puente J, Zaera R, Navarro C. An analytical model for high velocity impacts on thin CFRPs woven laminated plates. Int J Solids Struct 2007;44(9):2837-51.
[13]. López-Puente J, Varas D, Loya JA, Zaera R. Analytical modelling of high velocity impacts of cylindrical projectiles on carbon/epoxy laminates. Compos Part A Appl Sci Manuf 2009;40(8):1223-30.
[14]. Xia Y, Wang Y, Zhou Y, Jeelani S. Effect of strain rate on tensile behavior of carbon fiber reinforced aluminum laminates. Mater Lett 2007;61(1):213–5.
[15]. Zhou Y, Wang, Y., Jeelani S, Xia Y. Experimental study on tensile behavior of carbon fiber and carbon fiber reinforced aluminum at different strain rate. Appl Compos Mater 2007;14(1):17-31.
[16]. Naresh K, Shankar K, Rao B S, et al. Effect of high strain rate on glass/carbon/hybrid fiber reinforced epoxy laminated composites. Compos Part B Eng 2016;100:125-35.
[17]. TORAYCA® Prepreg, www.torayca.com/en/lineup/product/pro_003.html, 2017
[18]. Huang GY, Xu MM, Guo ZW, Feng SS. High velocity impact resistance of CFRP and carbon fiber-reinforced aluminum laminates. In: Proceedings of the Fifth International Symposium on Explosion, Shock wave and High strain-rate Phenomena. Beijing, China, September, 2016. p.70-1.
[19]. Ning H, Li Y, Hu N. Improvement of interlaminar mechanical properties of CARALL based on nanofiller interface reinforcement and other fabrication

techniques. In: Proceedings of 13th International Conference on Fracture. Beijing, China, June, 2013. p.1-11.

[20]. Xiong J, Zhang M, Stocchi A, Hu H, Ma L, Wu L, et al. Mechanical behaviors of carbon fiber composite sandwich columns with three dimensional honeycomb cores under in-plane compression. Compos Part B Eng 2014;60:350-8.

[21]. Breen C, Guild F, Pavier M. Impact of thick CFRP laminates: the effect of impact velocity. Compos Part A Appl Sci Manuf 2005;36(2):205-11.

[22]. Francesconi A, Giacomuzzo C, Kibe S, Nagao Y, Higashide M. Effects of high-speed impacts on CFRP plates for space applications. Adv Sp Res 2012;50(5):539-48.

[23]. Wen HM. Predicting the penetration and perforation of FRP laminates struck normally by projectiles with different nose shapes. Compos Struct 2000;49(3):321-9.

[24]. Ben-Dor, G., Dubinsky A, Elperin T., A model for predicting penetration and perforation of FRP laminates by 3-D impactors. Compos Struct 2002. 56(3): p. 243-8.

[25]. Ben-Dor G, Dubinsky A, Elperin T. A class of models implying the Lambent–Jonas relation. Int J Solids and Struct, 2001. 38(40): p. 7113-9.

[26]. Al-Shawaf A, Zhao XL. Adhesive rheology impact on wet lay-up CFRP/steel joints' behaviour under infrastructural subzero exposures. Compos Part B Eng 2013; 47:207-19.

Figures:

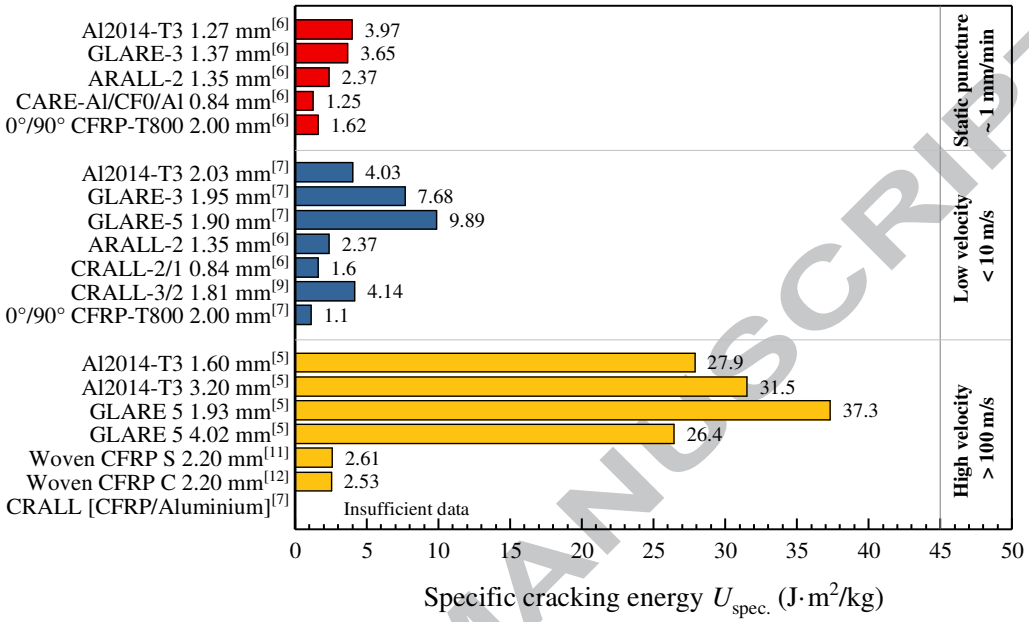

Fig. 1 Comparison of penetration resistance of FMLs

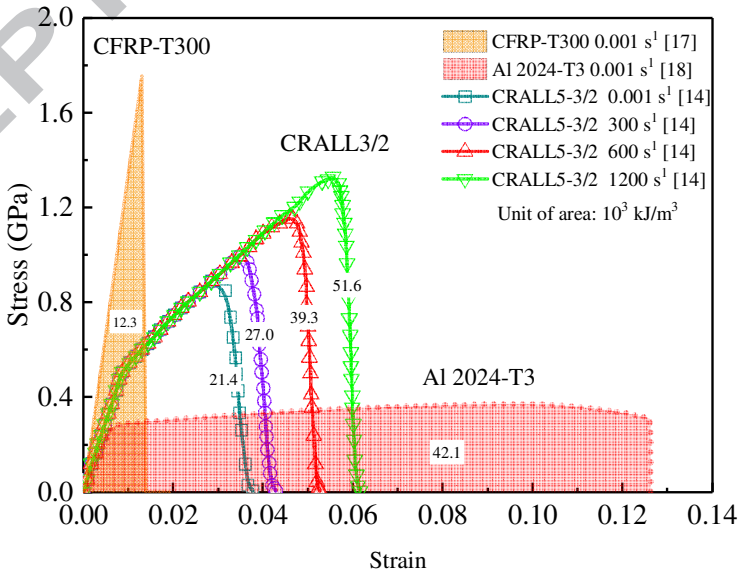

Fig. 2 Tensile stress–strain curves of T300, Al 2024-T3, and CRALLs

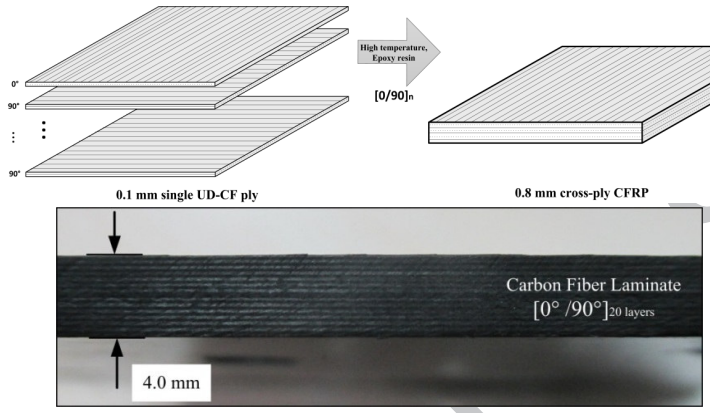

Fig. 3 Orthogonal laminated specimen of 4 mm T-700S Cross-ply CFRP

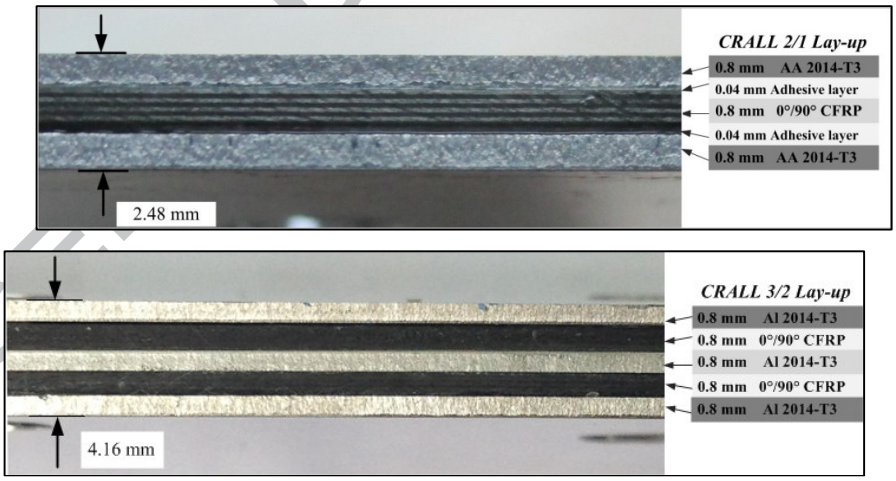

Fig. 4 Lay-up configuration of 2.48 mm CRALL2/1 and 4.16 mm CRALL3/2

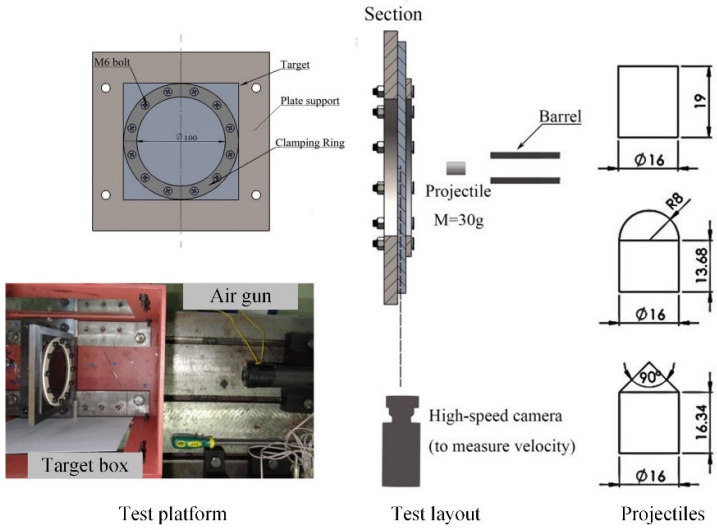

Fig. 5 Ballistic impact test arrangement and projectile geometries

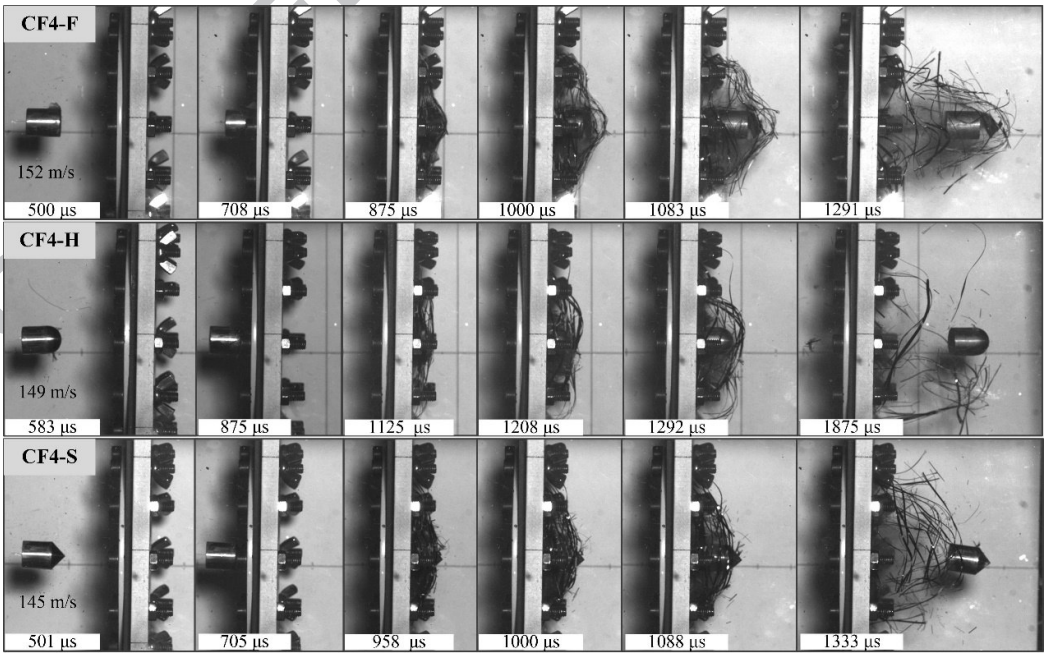

Fig. 6 Penetration process of CF4 target by projectiles

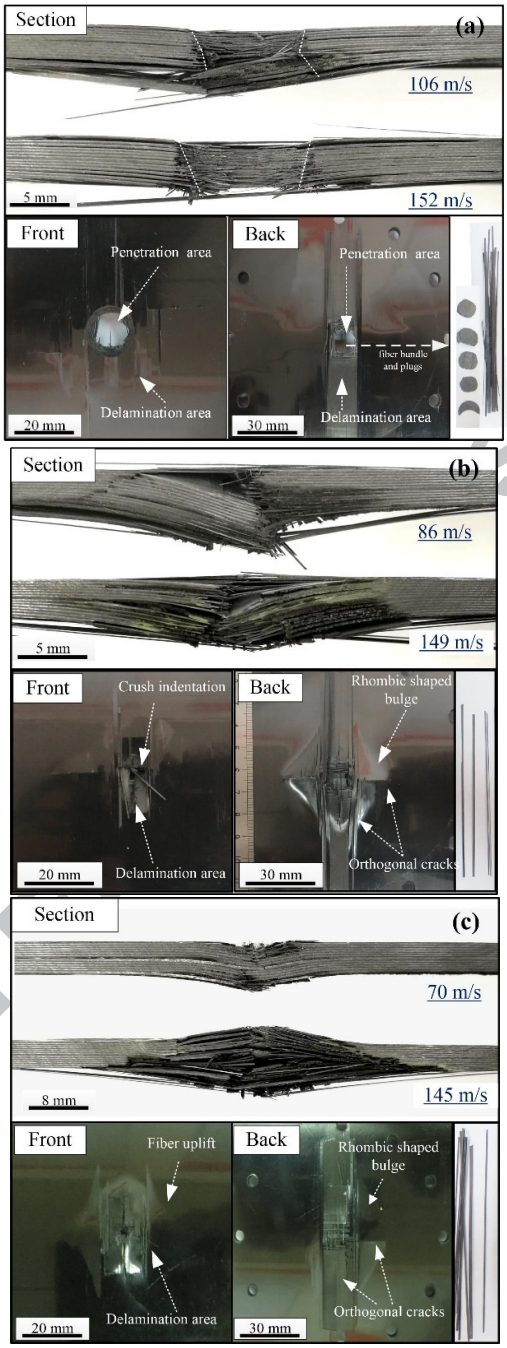

Fig. 7 Fracture mode of CF4 targets impacted by high velocity projectiles

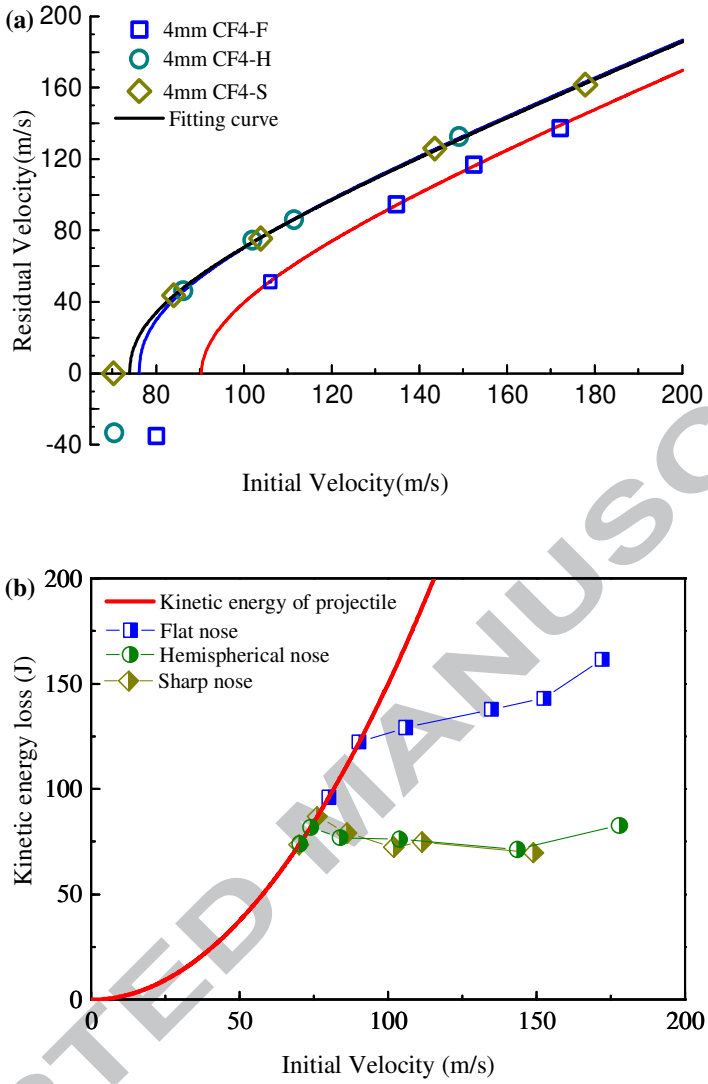

Fig. 8 ballistic limits and energy absorption of CFRP impacted by projectiles

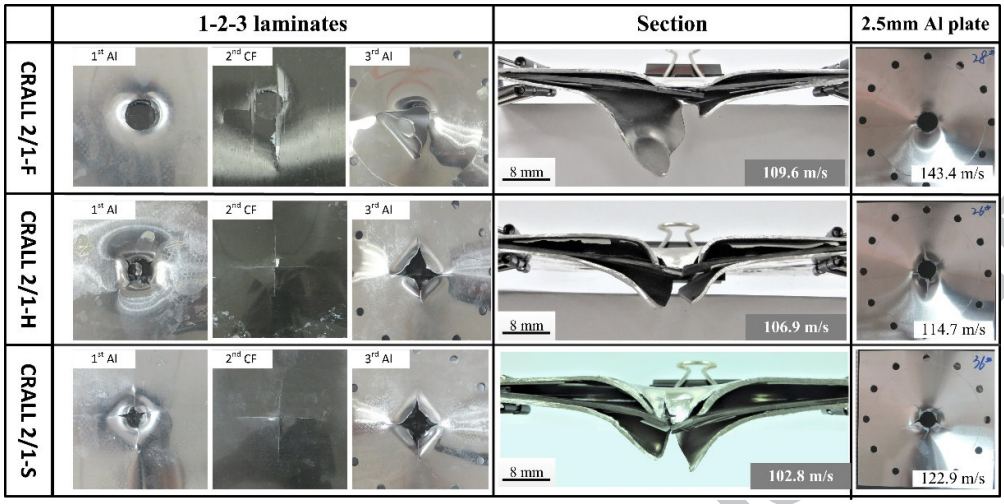

Fig. 9 Typical fracture modes of CRALL2/1 targets under projectiles impacting

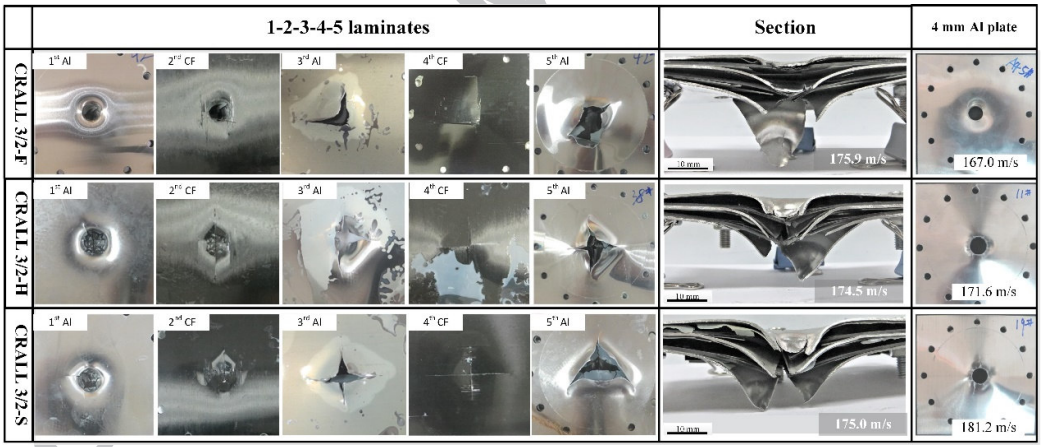

Fig. 10 Typical fracture modes of CRALL3/2 targets under projectiles impacting

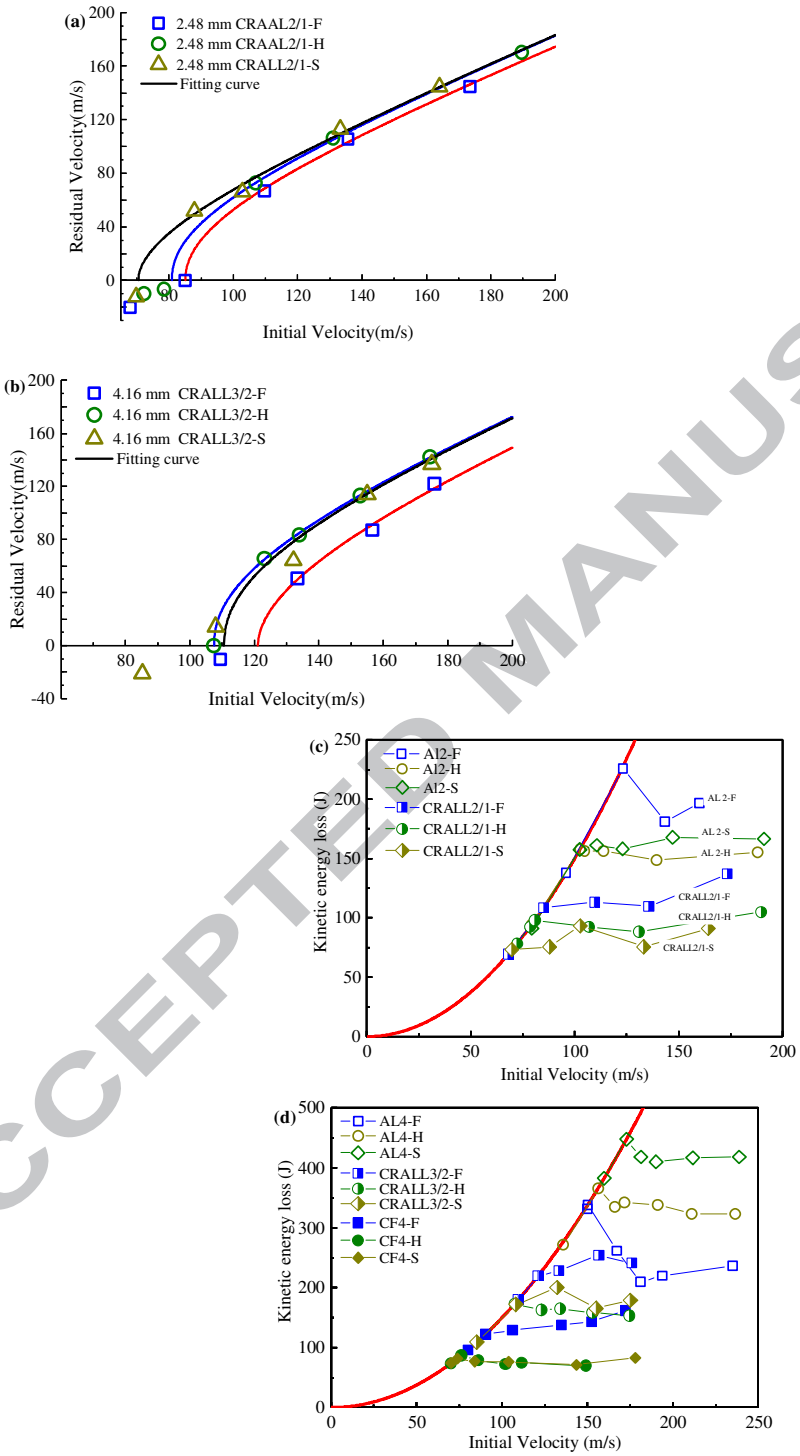

Fig. 11 Ballistic limits and energy absorption of CRALLs targets

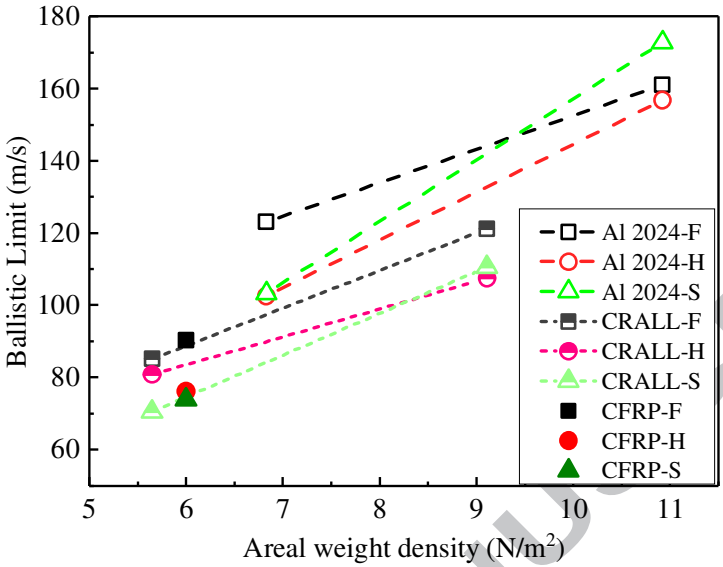

Fig. 12 Comparison of ballistic limits at same areal weight density

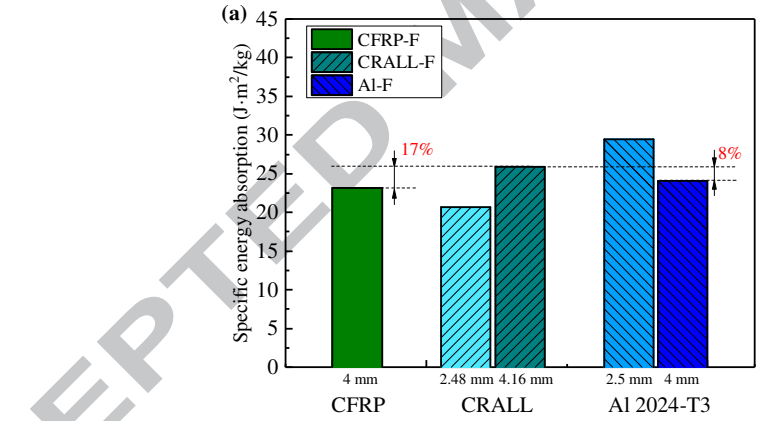

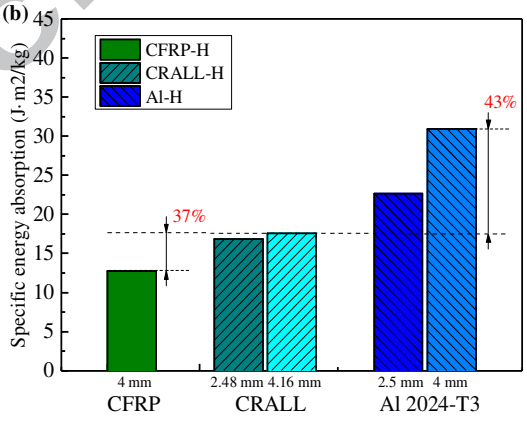

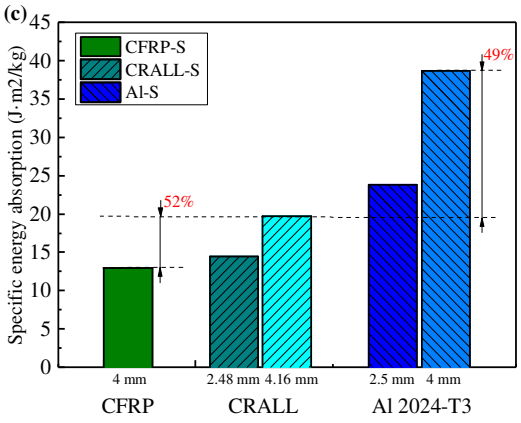

Fig. 13 The energy absorption of areal weight density after penetration

Tables:

Table 1 Static materials properties of unidirectional T-700S fibre/epoxy laminate

Properties	Value
Longitudinal stiffness, E_{11} (GPa)	135
Transverse stiffness, E_{22} (GPa)	10.3
Out-of-plane stiffness, E_{33} (GPa)	10.3
Poisson's ratio, $\tau_{12}=\tau_{31}$	0.25
Poisson's ratio, τ_{23}	0.38
Shear moduli, G_{12} (GPa)	6.5
Shear moduli, G_{13} (GPa)	6.5
Shear moduli, G_{23} (GPa)	3

	.91
Longitudinal tensile strength, Xt (MPa)	2
	550
Longitudinal compressive strength, X_c	1
(MPa)	050
Transverse tensile strength, Y_t (MPa)	2
	4
Transverse compressive strength, Y_c	1
(MPa)	32
Inter laminar shear strength, S (MPa)	7
	5
Out-of-plane tensile strength, Z_t (MPa)	6
	5
Density, ρ (kg/m^3)	1
	570

Table 2 Aluminium alloy 2024-T3 property

Property	Value
Elasticity modulus, E (GPa)	72.2

Poisson's ratio, τ	0.35
Yield stress, σ_y (MPa)	301
Ultimate tensile stress, σ_m(MPa)	372
Density, ρ (kg/m^3)	2750

Table 3 Description of CFRP, CRALLs and aluminium target panels

Material	Lay-up	Total thickness (mm)	Equivalent density ρ (g/cm3)
CFRP	$[0°/90°]_{40}$	4	1.57
CRALL3-2/1	Al/CF/Al	2.48	2.28
CRALL5-3/2	Al/CF/Al/CF/Al	4.16	2.19

Al 2014-T3	-	2.5	2.75
Al 2014-T3	-	4	2.75
Epoxy adhesive	-	0.04	1.10

Table 4 Summary of the impact resistance of CFRF, CRALLs and Al 2014-T3

Code	Areal weight density (kg/m^2)	Ballistic limit v_{bl} (m/s)	Average energy absorption $\Delta\bar{E}_k$ (J)	Specific energy absorption $\Delta\bar{E}_e$ ($J \cdot m^2/kg$)
CF4-F	6.28	90.3	138.8	22.11
CF4-H	6.28	76.1	76.6	12.77
CF4-S	6.28	73.9	77.8	12.97
CRALL3-F	5.65	85.2	117.1	20.71
CRALL3-H	5.65	80.9	95.2	16.84
CRALL3-S	5.65	70.5	81.7	14.45
CRALL5-F	9.11	121.1	235.8	25.88
CRALL5-H	9.11	107.5	159.8	17.54
CRALL5-S	9.11	110.6	179.3	19.68
Al2-F	6.88	123.0	201.2	29.24
Al2-H	6.88	102.5	154.9	22.51
Al2-S	6.88	103.3	162.2	23.58
Al4-F	11	161.3	263.1	23.92
Al4-H	11	156.8	337.7	30.70
Al4-S	11	172.8	422.1	38.37